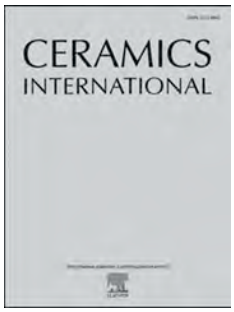

Effect of LMZBS glass on the microstructure and microwave dielectric properties of monocelsian ceramics

Mingxia Wang, Chaowei Zhong, Tianying Qin, Qiu Yang, Bin Tang, Shuren Zhang

PII: S0272-8842(20)30272-8

DOI: https://doi.org/10.1016/j.ceramint.2020.01.252

Reference: CERI 24184

To appear in: *Ceramics International*

Received Date: 25 December 2019

Revised Date: 22 January 2020

Accepted Date: 28 January 2020

Please cite this article as: M. Wang, C. Zhong, T. Qin, Q. Yang, B. Tang, S. Zhang, Effect of LMZBS glass on the microstructure and microwave dielectric properties of monocelsian ceramics, *Ceramics International* (2020), doi: https://doi.org/10.1016/j.ceramint.2020.01.252.

Effect of LMZBS Glass on the Microstructure and Microwave Dielectric Properties of Monocelsian Ceramics

Mingxia Wang[1,2], Chaowei Zhong[1,2*], Tianying Qin[1,2], Qiu Yang[1,2], Bin Tang[1,2], Shuren Zhang[1,2]

1. Key Laboratory of Multi-Spectral Absorbing Materials and Structures of Ministry of Education, University of Electronic Science and Technology of China, People's Republic of China.

2. School of Electronic Science and Engineering, University of Electronic Science and Technology of China, Chengdu, 610054, People's Republic of China.

[*] Corresponding author.

Emails: chaoweizhong1502@outlook.com

ABSTRACT

$BaAl_2Si_2O_8$-Li_2O-MgO-ZnO-B_2O_3-SiO_2 (BAS-LMZBS) glass ceramics were prepared through the solid-state route. The phase transformation, microstructure, bulk density and microwave dielectric properties of (1-x)$BaAl_2Si_2O_8$-xLMZBS(x=0.1-0.4) the glass ceramics were examined. The effects of the LMZBS additive as a mineralizer on the hexagonal-to-monoclinic transformation were investigated by X-ray diffraction and scanning electron microscope. All of the hexagonal phases were converted into monoclinic phases when x=0.1, and it was found that LMZBS glass affected the densification of the ceramic samples. Monocelsian was successfully prepared, and its sintering temperature was reduced from above 1400□ to 870□ by adding LMZBS glass. Excellent microwave dielectric properties (ε_r= 7.31, $Q \times f$ = 48926 GHz and τ_f = −48 ppm/°C) were obtained at 870□. This sample shows great chemical compatibility with Ag electrodes and can be a promising candidate for practical applications of low-temperature, co-fired ceramics.

KEYWORDS

LTCC; Phase transformation; Monocelsian; Hexacelsian; Microwave dielectric properties

1. Introduction

$BaAl_2Si_2O_8$ (BAS; Ba-Celsian) ceramics with a very high melting point (approximately 1760□) exist in three main kinds of crystal structures, namely monocelsian (monoclinic), hexacelsian (hexagonal) and α-hexacelsian (orthorhombic) [1, 2]. Hexacelsian is only thermodynamically stable between 1590□ and 1760□. Moreover, hexacelsian can exist as a metastable structure between 25□ and 1590□, and the hexagonal phase can be reversibly transformed to an orthorhombic phase at 300□; this transformation is accompanied by a volume change of 3% and usually gives rise to microcracks in the sample [3]. By contrast, monocelsian is thermodynamically stable below 1590□. The monoclinic phase is more popular for applications such as resonators, filters, and dielectric antennas for microwave components and as a substrate for electronic applications [4] due to its good thermal properties, low permittivity, good oxidation resistance and low thermal expansion coefficient [5, 6].

Monocelsian as the most desirable crystal phase in microwave dielectric materials. According to previous reports, many methods have been used to synthesize monocelsian, such as traditional glass-ceramic processing, the sol–gel method, and the calcination of oxide mixtures. However, regardless of the method used, hexacelsian was consistently observed to be the first phase to nucleate. The complete transformation to the monoclinic from hexacelsian is very sluggish [7]. In previous research, it was found that the phase transformation from hexagonal to monoclinic can be achieved by using mineralizers or by raising the sintering temperature. Shirooyeh et al found that the addition of 5 mol% Y_2O_3 could promote the full transformation of hexagonal to monoclinic within 4 h at 1350□ [8]. In another work, using a three-step firing technique, Li et al synthesized monocelsian at sintering temperatures between 1200 and 1530□ [3]. Yang et al found that the addition of 0.05 mol of Ca enabled the successful synthesis of monocelsian at 1425□ with ε_r = 6.7, $Q \times f$ =24335 GHz and τ_f =19.3 ppm/ °C [1]. Huang et al successfully promoted the full conversion from hexagonal to monoclinic, while reducing the sintering temperature slightly to 950□ by adding Li_2O-B_2O_3 glass, and obtained properties of ε_r

= 6.3, $Q \times f$ = 24366 GHz, and τ_f = -27.4 ppm/ °C [9]. Although these experiments demonstrated the successful synthesis of monocelsian, the high sintering temperature and poor dielectric properties limit their use in practical applications. To date, there have been few reports on monocelsian ceramic materials in the LTCC field with excellent dielectric properties.

Song et al. studied the effects of ZnO and SiO_2 on the BAS materials. The results showed that ZnO and SiO_2 can significantly reduce the sintering temperature and stabilize the phase structure [10]. Huang et al reported the phase transformation from hexagonal to monoclinic using Li_2O-B_2O_3 as the additive [9]. These results show that an appropriate amount of Li_2O-B_2O_3 can effectively promote the hexagonal-to-monoclinic transformation. According to the theory of glass formation, an appropriate amount of an alkali metal oxide, such as Li_2O, Na_2O, and K_2O, is added to the SiO_2 or H_3BO_3 glass. The oxygen atoms in the alkali metal oxide are connected to the Si atom, and this alkali metal ion breaks the bridge connection to produce non-bridged oxygen atoms. This connection leads to the lower viscosity of the solution and ensures its easier flow, reducing the glass softening point. A study of the effects of LMZBS glass on the $BaAl_2Si_2O_8$ ceramics has not been reported. To evaluate the effects of this additive on the hexacelsian-to-monocelsian transformation, different proportions of LMZBS glass were used as the additive in this work. Additionally, the effect of LMZBS glass on the phase composition, microstructure, bulk density, and microwave dielectric properties were systematically examined in terms of the LMZBS glass content and sintering temperature.

2. Experimental procedures

$BaCO_3$, Al_2O_3 and SiO_2 high purity powders provided by CHRON CHEMISTRY were weighed according to the stoichiometric ratio of $BaAl_2Si_2O_8$ and then ball-milled in a nylon jar with ZrO_2 balls for 5 h using deionized water as a medium. The dried mixture was calcined at 1250□ for 4 h in air. Li_2CO_3, MgO, ZnO, H_3BO_3 and SiO_2 high-purity powders provided by CHRON CHEMISTRY were weighed and used in the amounts shown in Tab. 1 to prepare LMZBS glass, and then the mixture was melted at 1400□ and quenched in deionized water.

Powders with different mass ratios (1-*x*)BAS-*x*LMZBS (*x*=0.1-0.4) were milled with ZrO_2 balls in a nylon jar for 5 h using deionized water as the medium. It was shown experimentally that the sample cannot be densified by sintering for $x < 0.1$. Therefore, this work only reports the relevant data for the samples could be densified by sintering. The mixed powder was ground into granules and then pressed into pellets (15 mm×7 mm). Then, the pellets were sintered at 850□, 870□, 900□, 930□, 960□, and 990□ for 4 h at a rate of 2□/min.

The phase transformation was investigated by X-ray diffraction analysis (XRD, DX-1000 CSC, Japan). The microstructure of the sample surface was observed by scanning electron microscopy (SEM; FEI Inspect F). The elemental content was measured by EDS (JSM-6490LV). The bulk density was measured by the Archimedes method. The dielectric properties were obtained by the Hakki-Coleman dielectric resonator method (HP83752A, USA). The τ_f values were calculated by the following formula:

$$\tau_f = \frac{f_{85} - f_{25}}{f_{25} \times (85 - 25)} \quad (1)$$

where f_{25} and f_{85} are the resonant frequencies at 25□ and 85□, respectively.

3. Results and discussion

3.1 Effect of LMZBS glass on the phase transformation

Fig. 1(a) shows the lattice structure of the hexacelsian. It is observed from Fig. 1(a) that the hexacelsian is an infinite two-dimensional hexagonal thin-layer structure that is connected by the common vertices of the tetrahedra. The tetrahedra of each layer shares three vertices, and the remained vertices have the same oxygen arrangement. Two tetrahedral layers extending infinitely in two dimensions form a two-layer hexagonal layered structure through the sharing of the remaining oxygen atoms. The Ba^{2+} ions are located between the two layers for charge balance. There are twelve equidistant O^{2-} ions around the Ba^{2+} ion [6, 11-15]. The monocelsian is a three-dimensional frame structure shown in Fig. 1(b), with a single structural unit composed of eight tetrahedra connected together. The Ba^{2+} are randomly distributed in the tetrahedral network voids for charge balance. There are ten adjacent O^{2-} ions

around the Ba^{2+} ion located at different distances from the Ba^{2+} ion [16].

LMZBS glass contains Li^{+} (CN=4), Mg^{2+}(CN=4), Zn^{2+}(CN=4), and B^{3+}(CN=6) with the ionic radii of ~0.59 Å, ~0.57 Å, ~0.60 Å, and ~0.27 Å, respectively. The void sizes of the D6R (double six membered-rings-of-tetrahedra) interstitial site and the S4R (single four-membered-ring) interstitial site calculated from the interatomic distances in hexacelsian were reported by Yoshiki and Matsumoto as ~1.90 and ~0.37 Å, respectively. The other interstitial site in hexacelsian is the S6R (single six-membered-ring) site that is already occupied by the host Ba^{2+} ion. After the LMZBS glass is dissolved in the hexacelsian crystal, the ions in the glass can only occupy five positions, namely, the original Ba, Al, and Si positions, D6R and S4R [2, 17, 18] [19, 20].The radius of Li^{+} is larger than that of Al^{3+} (CN=4, R=0.39A), and analysis shows that some of the Li^{+} may occupy the Al sites. Due to the charge difference between Al^{3+} and Li^{+}, oxygen vacancies are generated to compensate for the charge imbalance. The chemical equation of the defect reaction is given by [6]:

$$Li_2O = 2Li_{Al}^{''} + 2V_o^{\square} + O_o^{\times} + V_{BaSi_2O_5}^{\times}$$

In addition, since the ionic diameter of Li^{+} is smaller than the size of D6R, it is known that some of the Li^{+} ions may also be incorporated into the void of D6R; in addition, Ba^{2+} vacancies are generated to compensate for the defects. The formation of the doped solid solution promoted the transformation of the hexagonal phase to the monoclinic phase. The chemical equation of the defect reaction is given by:

$$Li_2O = 2Li_i^{\square} + V_{Ba}^{''} + O_o^{\times} + V_{Al_2Si_2O_7}^{\times}$$

The Mg^{2+} and the Zn^{2+} have the charge, and their ionic radii are only slightly different. Due to the charge difference between Mg^{2+}, Zn^{2+} and Al^{3+}, oxygen vacancies are also generated to compensate for the charge imbalance. In this case, the chemical equation of the defect reaction is given by [6, 21]:

$$2MgO = 2Mg_{Al}^{'} + V_o^{\square} + 2O_o^{\times} + V_{BaSi_2O_5}^{\times}$$

$$2ZnO = 2Zn_{Al}^{'} + V_o^{\square} + 2O_o^{\times} + V_{BaSi_2O_5}^{\times}$$

In addition, since the diameters of the Zn^{2+} and Mg^{2+} ions are smaller than the size of

D6R, some of the Zn^{2+} and Mg^{2+} ions may also be incorporated into the D6R; in addition, Ba^{2+} vacancies are generated to compensate for the defects. In this case, the chemical equation of the defect reaction is given by:

$$MgO=Mg_i^{\boxtimes}+V_{Ba}^{''}+O_o^{\times}+V_{Al_2Si_2O_7}^{\times}$$

$$ZnO=Zn_i^{\boxtimes}+V_{Ba}^{''}+O_o^{\times}+V_{Al_2Si_2O_7}^{\times}$$

The O vacancies or Ba vacancies generated by the addition of the Mg^{2+}, Li^{+}, and Zn^{2+} ions promote the breaking of the Ba-O, Al-O and Si-O bonds, reforming the $Al(Si)O_4$ tetrahedra into a three-dimensional frame structure, and promoting the transformation of hexacelsian into monocelsian [12, 22]. The main role of Si^{4+} is to form an irregular continuous network of the $[SiO_4]$ tetrahedral structural units in the glass; this network then becomes the skeleton of the glass. For B^{3+}, $[BO_3]$ and $[BO_4]$ are the structural units, and this unit structure, together with $[SiO_4]$, forms the structural network of the glass. In addition, H_3BO_3 can act as a cosolvent that can accelerate the vitrification of the glass [23]. The existence of anion and cation vacancies may promote the transformation because these vacancies increase the energy of hexacelsian and reduce the activation energy of the transformation.

3.2 Analysis of XRD data

The XRD patterns of the (1-*x*)BAS-*x*LMZBS (*x* = 0, 0.1, 0.2, 0.3, 0.4) samples sintered at 870□ with different compositions are shown in Fig. 2(a). It is observed from Fig. 2(a) that all of the diffraction peaks were found to match the hexagonal $BaAl_2Si_2O_8$ with no second phase at *x*=0. As *x* = 0.1, three phases begin to appear, and the observed diffraction peaks were indexed as monocelsian (PDF#38-1450), $Mg_2B_2O_5$ (PDF#86-0531) and Li_2ZnSiO_4 (PDF#24-0677) phases. It is observed that the LMZBS glass can effectively promote the phase transformation from the hexagonal phase to the monoclinic phase. Moreover, a magnified view of the XRD patterns for the 2θ range of 18°-35° is presented in Fig. 2(b) for a further examination of the diffraction peaks, with the oblique lines in Fig. 2(b) representing a discontinuity in the graph. With the increase in the LMZBS glass content, at 2θ = 19.834°, the $Mg_2B_2O_5$ peak gradually increased. At 2θ = 33.026°, the intensity of the Li_2ZnSiO_4

peak also increased, suggesting that increase in the $Mg_2B_2O_5$ and Li_2ZnSiO_4 contents with increasing glass content. Furthermore, the XRD patterns of the (1-*x*)BAS-*x*LMZBS (*x*=0.3) samples sintered at different temperature between 850°C and 930°C are also shown in Fig. 2(b). As expected, the phase compositions remained unchanged, with the main crystalline monocelsian and secondary $Mg_2B_2O_5$ phases coexisting with a small amount of Li_2ZnSiO_4 dioxide. It is concluded that the LMZBS glass can effectively affect the formation of monoclinic $BaAl_2Si_2O_8$.

3.3. Scanning electron micrograph analysis

Figs. 3(a)–(d) show the surface morphology of the (1-x)BAS-xLMZBS(x = 0.1-0.4) ceramics sintered at 870°C for 4 h. As shown in Figs. 3(a) and (b), the samples exhibited many matrix grains and stick-like grains, and a small number of pores were also observed. It is observed from Fig. 3(c) that the stick-like grains start to grow with less pores, and many small granule grains appear. After *x*=0.3, the ceramic surface shows a large amount of the liquid phase as excess LMZBS content that inevitably affects the bulk density and the dielectric loss. Therefore, it is clear that a suitable LMZBS content can effectively affect the sintering temperature of the ceramic samples, and it is concluded from Fig. 3(c) that the optimal densification effect can be obtained at *x*=0.3. Figs. 3(e)–(h) show the surface morphology of the 0.7BAS-0.3LMZBS sintered at 850□-960□. It is clearly observed that the degree of densification first increased and then decreased as the sintering temperature was raised from 850□ to 960□. The change in the densification shows that the optimal sintering temperature was 870□. As observed from Figs. 3(f) and (i), it is important to note that the number of pores increases with increasing temperature from 900□, which may be ascribed to the volatilization of Li_2O and B_2O_3 on the ceramic surface [24] [25] and overfiring.

EDS measurements were performed to investigate the chemical elements' distribution of the A, B and C spots indicated in Figs. 3(b) and 3(c) for *x*=0.2-0.3. The EDS results for the indicated areas are shown in Fig. 4. The results show that all of the spots contain the O, Mg, Al and Si elements, and this may be due to the presence of three phases of $Mg_2B_2O_5$ (PDF#86-0531), monocelsian (PDF#38-1450), and

Li_2ZnSiO_4 (PDF#24-0677)) in the sample according to the XRD analysis. Furthermore, Fig. 4(a) shows that the Mg: O ratio is close to 2: 5 in spot A (the stick-like grain), further proving the existence of the $Mg_2B_2O_5$ phase. In addition, Fig. 4(b) shows that the Ba: Al: Si: O ratio in spot B (the matrix particles) was close to 1: 2: 2: 8, indicating the formation of the monocelsian (PDF#38-1450) phase. As the glass content increases, small crystal granules appear in Fig. 3(c), and Fig. 4(c) shows that spot C (small agglomerated granule grains) is rich in Zn, Al and O elements, which may be attributed to the Li_2ZnSiO_4 (PDF#24-0677) phase. It can be surmised that the presence of Al in spot C can be explained by the small agglomerated granule grains attached to the large matrix particles (monocelsian). Additionally, Mg can be detected in all the regions, possibly due to the wide distribution of the $Mg_2B_2O_5$ phase in the sample. Combining these results with the results of the XRD analysis, it is concluded that the matrix particles, the stick-like grains and the small agglomerated granule grains are monocelsian, $Mg_2B_2O_5$ and Li_2ZnSiO_4, respectively. The results obtained by EDS are consistent with the XRD results.

3.3. Microwave dielectric properties of (1-*x*)BAS-*x*LMZBS glass-ceramic

The change in the bulk density was calculated according to:

$$D = \frac{\sum_{i=1}^{n} W_i}{\sum_{i=1}^{n} W_i / D_i} \quad (2)$$

where n represents the number of the phases of the sample, and W_i represents the weights of the different components with densities D_i. The bulk densities of the various phases are presented in Tab. 2. The densities of the LMZBS glass, $Mg_2B_2O_5$ and Li_2ZnSiO_4 were 2.35 g/cm^3 [26], 2.91 g/cm^3, and 3.51 g/cm^3, respectively. Fig. 5(a) displays the bulk density as a function of x for the samples basically sintered at the temperatures in the 850-960□ range. It is observed that both the sintering temperature and LMZBS content have a significant effect on the bulk density of the (1-*x*)BAS-*x*LMZBS samples. For all of the (1-*x*)BAS-*x*LMZBS samples, the body density first increases and then decreases with increasing temperazture. The initial increase in the bulk density may be responsible for the decline in the porosity. However, the subsequent decrease in the density can be ascribed to the pores caused

by the volatilization of the Li_2O and B_2O_3 gas; this is consistent with the SEM images presented in Figs. 3(f)-(h). For sintering at 870□, the difference in the bulk density of the (1-*x*)BAS-*x*LMZBS(*x*=0.1-0.3) samples appears to be very small, which is consistent with the results of the SEM analysis presented in Figs. 3(a)-(c) that show that all of the samples exhibit higher densification. In addition, the bulk density showed a clear decrease at *x*=0.4, which can be explained by the liquid phase shown in Fig. 3(d).

Generally, the ε_r value of the sample can be expressed according to the following mixing rule:

$$\ln \varepsilon_r = x_1 \ln \varepsilon_{r_1} + x_2 \ln \varepsilon_{r_2} + \cdots + x_i \ln \varepsilon_{r_i} \quad (3)$$

where ε_{ri} and x_i are the permittivity and volume fraction of phase *i*, respectively. It is well-known that the increase in the pores will inevitably lead to the decrease in the dielectric constant of the samples because the dielectric constant of air is equal to 1. When the (1-*x*)BAS-*x*LMZBS samples were sintered at the same temperature, the dielectric constant decrease linearly with increasing LMZBS glass content. This result occurred due to the increase in the content of the Li_2ZnSiO_4 and $Mg_2B_2O_5$ phases that have low dielectric constants (according to Tab. 2). For 0.7BAS-0.3LMZBS, the dielectric constant first increases and then decreases with increasing sintering temperature, and finally, a slight increase in the dielectric constant is observed for sintering at 960□. It is observed from Figs. 5(a) and (b) that the trends observed for the dielectric constant are consistent with the trends observed for the bulk density for the temperatures <930□. Furthermore, the increase in the dielectric constant in the first stage may be owing to the reduction in the pore sizes with increasing sintering temperature, while the subsequent decrease is due to the low dielectric constants of the Li_2ZnSiO_4 and $Mg_2B_2O_5$ phases. The final slight increase may be attributed to the increased sintering densification, which is consistent with the SEM analysis results presented in Fig. 3(h).

Fig. 5(c) presents the $Q \times f$ values obtained for all of the samples. It is observed that the $Q \times f$ value exhibits the same trend as the bulk density. The $Q \times f$ values for the

(1-*x*)BAS-*x*LMZBS samples sintered at the same temperature first increase and then decrease with increasing LMZBS content. The increase in the *Q*×*f* value is due to the increased densification of the samples. Meanwhile, the dielectric loss values for the different phases can also affect the *Q*×*f* values of the ceramics. Because the *Q*×*f* value of the pure monocelsian phase (62190) is much higher than the *Q*×*f* values of Li_2ZnSiO_4 (14700) and $Mg_2B_2O_5$ (32100) as shown in Tab. 2, the addition of the glass will lead to a large dielectric loss. Therefore, with increasing LMZBS content, the *Q*×*f* value of (1-*x*)BAS-*x*LMZBS glass-ceramic will inevitably decrease. The *Q*×*f* values of the 0.7BAS-0.3LMZBS samples sintered at different temperatures first increase and then decrease with increasing sintering temperature. For the sample sintered at 870□, the SEM image presented in Fig. 3(c) shows that the sample exhibits higher densification, leading to higher *Q*×*f* values. The *Q*×*f* value is influenced not only by the *Q*×*f* value of each constituent phase but also by the crystal defects, grain boundary size, grains size and porosity. As the sintering temperature increases, the grain uniformity and the pores caused by the volatilization of Li_2O and B_2O_3 gas also contributed to the decreasing trend observed for the *Q*×*f* values. For these reasons, the *Q*×*f* value varies between 15093 and 48926.

Fig. 6 illustrates the dielectric properties of (1-*x*)BAS-*x*LMZBS sintered at 870□ for 4 h. For the glass contents in the x = 0.1-0.3 range, all of the samples exhibit a high degree of densification. As the glass content increase further, the bulk density decreased drastically due to the existence of a large amount of liquid glass. The increase in the ε_r value is due to the decrease in the porosity obtained with a slight increase in the sintering temperature, while the reduction in the ε_r value is due to the lower ε_r values of both Li_2ZnSiO_4 and $Mg_2B_2O_5$. The *Q*×*f* value of the samples first increases and then decreases, which is caused by the reduction of the pores and the increase in the glass content that lead to a large dielectric loss. The τ_f value decrease from -41.0 ppm/□ to -56.0 ppm/□ with increasing x. As shown in Tab. 2, all of the compositions have negative τ_f values [27] [28]. It is inferred that LMZBS glass has a more negative τ_f value. In summary, the excellent microwave dielectric properties of ε_r =7.3, τ_f = - 48.0 ppm/□, and *Q*×*f* = 48926 can be obtained for the 0.7BAS-

0.3LMZBS sintered at 870□ for 4 h. In this experiment, hexacelsian transformed into monocelsian at a relative low temperature of 870□ with a high $Q\times f$ value of 48926.

Fig. 7 illustrates the process of the monocelsian formation. The formation of (1-*x*)BAS-*x*LMZBS glass ceramic can be decomposed into four processes of particle rearrangement, LMZBS glass softening and hexacelsian particle dissolution, viscosity flow and bonds breaking, and monocelsian crystallization. Under the driving force provided by the LMZBS glass [29], the formation of the monocelsian phase was ascribed to the O vacancies or Ba vacancies generated by the addition of the LMZBS glass that promotes the breaking of the Ba-O, Al-O and Si-O bonds of hexacelsian.

We then examined the chemical compatibility of the sample with the Ag electrode. The co-firing of 0.7BAS-0.3LMZBS with Ag was carried out at 870□ for 4 h. The cross-section mapping area scan of the co-fired 0.7BAS-0.3LMZBS is shown in Fig. 8. It is observed that there was no obvious chemical reaction between the sample and Ag, and Ag did not diffuse in the 0.7BAS-0.3LMZBS during the process. Thus, this system combines the superior microwave dielectric properties of 0.7BAS-0.3LMZBS and the stable chemical compatibility of Ag. The comparison of our system with others low-permittivity LTCC ceramics is shown in Tab. 3 [1, 30-34] [25, 35-40]. It is observed that 0.7BAS-0.3LMZBS glass ceramics have lower sintering temperatures, low ε_r values and high $Q\times f$ characteristics, so this ceramic can is an excellent material for LTCC devices.

Conclusion

It this paper, the traditional solid-state method was used to synthesize monocelsian glass ceramics from the $BaCO_3$-Al_2O_3-SiO_2 (BAS) ternary mixture and LMZBS glass.

(1) The ions in the LMZBS glass enter either the Al position or the D6R gap position, generating O vacancies or Ba vacancies; this promotes the breaking of Ba-O, Al-O and Si-O bonds, reconnecting [Al(Si)O_4] tetrahedrons into a three-dimensional frame structure and promoting the transformation of hexacelsian into monocelsian.

(2) The sintering temperature of monocelsian ceramics was decreased from above 1400□ to 870□ by the addition of LMZBS glass. The XRD results show that

LMZBS glass crystallized forming $Mg_2B_2O_5$ and Li_2ZnSiO_4, and did not react with BAS ceramics. This work shows that an appropriate LMZBS content can promote the phase transformation from hexacelsian to monocelsian.

(3) The addition of an appropriate amount of the LMZBS sintering aid promotes the crystal growth and improves the densification of ceramics, improving the microwave dielectric properties of BAS ceramics. For the samples with 0.7BAS-0.3LMZBS sintered at 870 □, microwave dielectric properties (ε_r= 7.3, $Q\times f$ = 48926 GHz and τ_f = -48.0 ppm/°C) suitable for use in practical devices were obtained.

Acknowledgments

We thank the National Natural Science Foundation of China (No. 51272035) for its strong support of this work.

References

[1] X. Yang, Y. Zhang, S. Ding, L. Huang, X. Zhang , Structure and dielectric properties of Ca doped $BaAl_2Si_2O_8$, Ceram. Int. 44 (2018) 43-45.
[2] B. Yoshiki, K. Matsumoto, High-Temperature Modifkation of Barium FeIdspar, J. Am. Ceram. Soc. 34 (1951) 283-286.
[3] Q. Li, D. Cai, Z. Yang, X. Duan, P. He, Y. Sun, H. Li, D. Jia, Y. Zhou, Thermal properties and thermal shock resistance of BAS-BN composite ceramics, Ceram. Int. 45 (2019) 8181-8187.
[4] C.M. López-Badillo, J. López-Cuevas, C.A. Gutiérrez-Chavarría, J.L. Rodríguez-Galicia, M.I. Pech-Canul, Synthesis and characterization of $BaAl_2Si_2O_8$ using mechanically activated precursor mixtures containing coal fly ash, J. Eur. Ceram. Soc. 33 (2013) 3287-3300.
[5] A.S. Radosavljević-Mihajlović, M.D. Prekajski, J. Zagorac, A.M. Došen, S.S. Nenadović, B.Z. Matović, Preparation, structural and microstructural properties of $Ba_{0.64}Ca_{0.32}Al_2Si_2O_8$ ceramics phase, Ceram. Int. 38 (2012) 2347-2354.
[6] K.T. Lee, P.B. Aswath, Role of mineralizers on the hexacelsian to celsian transformation in the barium aluminosilicate (BAS) system, Mater. Sci. Eng., A. 352 (2003) 1-7.
[7] Y. Kobayashi, Transformation kinetics from hexacelsian to celsian for powders having uniform particle size, Ceram. Int. 27 (2001) 179-184.
[8] M. Shirooyeh, A. Nemati, The Effect of Y_2O_3 Additive on the Formation of Monoclinic Celsian, 2005.
[9] L. Huang, S. Ding, X. Yan, T. Song, Y. Zhang, Structure and microwave dielectric properties of $BaAl_2Si_2O_8$ ceramic with Li_2O–B_2O_3 sintering additive, J. Alloys Compd. 820 (2020).
[10] X. Song, W. Lu, X. Wang, G. Fan, R. Muhammad, W. Lei, Sintering behaviour

and microwave dielectric properties of $BaAl_{2-2x}(ZnSi)_xSi2O8$ ceramics, J. Eur. Ceram. Soc. 38 (2018) 1529-1534.
[11] E.A.M. El-Meliegy, S.A.M. Abdel-Hameed, Enstatite–celsian glass ceramics, Mater. Charact. 55 (2005) 28-34.
[12] K.T. Lee, Kinetics of the hexacelsian to celsian transformation in barium aluminosilicates doped with CaO, Int. J. Inorg. Mater. 3 (2001) 687-692.
[13] Y. Sung, Crystallization of celsian glasses of $(SrO\text{-}Al_2O_3\text{-}2SiO_2)$–$(Al_2O_3)$ pseudobinary compositions, J. Mater. Sci. Lett. 20 (2001) 839-840.
[14] Y. Sung, Sintering and crystallization of off-stoichiometric $BaO\text{-}Al_2O_3\text{-}2SiO_2$ glasses, Asian J. Mater. Sci. 35 (2000) 4913-4918.
[15] S. BosÏkovicÂ, Synthesis of Si_3N_4–celsian composite materials, Ceram. Int. 26 (2000) 33-37.
[16] Y. Takeuchi, A DETAILED INVESTIGATION OF THE STRUCTURE OF HEXAGONAL BaA12Si2O8 WITH REFERENCE TO ITS INVERSION, MINERAL MAG. 2 (1958) 311-332.
[17] N. Curetti, P. Benna, E. Bruno, High-pressure structural configuration and phase transition in celsian, $BaAl_2Si_2O_8$, Phys. Chem. Miner. 44 (2016) 181-192.
[18] T.M.Y. Goto, formation process of sr-celsian from precursor zeolites, J. Ceram. Soc. Jpn. 117 (2009) 748-752.
[19] G.K. Savchuk, T.P. Petrochenko, A.A. Klimza, Preparation and dielectric properties of celsian ceramics based on hexagonal $BaAl_2Si_2O_8$, Inorg. Mater. 49 (2013) 632-637.
[20] B. Yoshiki, K. Matsumoto, High-Temperature Modifkation of Barium FeIdspar, J. Am. Ceram. Soc. 34 (1951) 283-286.
[21] B. Li, M. Xu, B. Tang, Effects of ZnO on crystallization, microstructures and properties of BaO–Al_2O_3–B_2O_3–SiO_2 glass–ceramics, J. Mater. Sci. - Mater. Electron. 27 (2015) 70-76.
[22] T. Sun, H. Xiao, W. Guo, X. Hong, Effect of Al_2O_3 content on BaO–Al_2O_3–B_2O_3–SiO_2 glass sealant for solid oxide fuel cell, Ceram. Int. 36 (2010) 821-826.
[23] Y. Zhou, C. Chang, A. Inoue, Effect of B to Si concentration ratio on glass-forming ability and soft-magnetic properties in $(Co_{0.705}Fe_{0.045}B_{0.25-x}Si_x)_{96}Nb_4$ glassy alloys, J. Appl. Phys. 101 (2007) 09N101-109N101.
[24] M.M. Krzmanc, M. Valant, D. Suvorov, The synthesis and microwave dielectric properties of $Sr_xBa_{1-x}Al_2Si_2O_8$ and $Ca_yBa_{1-y}Al_2Si_2O_8$ ceramics, J. Eur. Ceram. Soc. 27 (2007) 1181-1185.
[25] T. Joseph, M.T. Sebastian, H. Sreemoolanadhan, V.K. Sree Nageswari, Effect of Glass Addition on the Microwave Dielectric Properties of $CaMgSi_2O_6$ Ceramics, Int. J. Appl. Ceram. Technol. 7 (2009) 98-106.
[26] X. Du, H. Su, H. Zhang, Z. Zhou, Y. Jing, G. Gan, X. Tang, High-Q microwave dielectric properties of $Li(Zn_{0.95}Co_{0.05})_{1.5}SiO_4$ ceramics for LTCC applications, Ceram. Int. 43 (2017) 7636-7640.
[27] L. Xie, C. Zhong, Z. Fang, Y. Zhao, B. Tang, S. Zhang, Microwave dielectric properties of $Li_2O\text{-}xMgO\text{-}ZnO\text{-}B_2O_3\text{-}SiO_2$ glass-ceramics (x = 30-50 wt.%), J. Ceram. Soc. Jpn. 126 (2018) 163-169.

[28] K.P. Surendran, M.T. Sebastian, M.V. Manjusha, J. Philip, A low loss, dielectric substrate in $ZnAl_2O_4$–TiO_2 system for microelectronic applications, J. Appl. Phys. 98 044101 (2005).
[29] R.R. Turnmala, Ceramic and Glass-Ceramic Packaging in the 1990s, J. Am. Ceram. Soc. 5 (1991) 895-908.
[30] X. Song, K. Du, Z. Zou, Z. Chen, W. Lu, S. Wang, W. Lei, Temperature-stable $BaAl_2Si_2O_8$–$Ba_5Si_8O_{21}$ based low-permittivity microwave dielectric ceramics for LTCC applications, Ceram. Int. 43 (2017) 14453-14456.
[31] X. Chen, F. Wang, W. Zhang, Low temperature sintering and dielectric properties of La_2O_3–B_2O_3–Al_2O_3 glass–ceramic/Al_2O_3 composites for LTCC applications, J. Mater. Sci. - Mater. Electron. 30 (2019) 3098-3106.
[32] T. Qin, C. Zhong, H. Yang, Y. Qin, S. Zhang, Investigation on glass-forming ability, Flexural strength and microwave dielectric properties of Al_2O_3-doped LMZBS glasses, Ceram. Int. 45 (2019) 10899-10906.
[33] S. Thomas, M.T. Sebastian, Effect of B_2O_3-Bi_2O_3-SiO_2-ZnO glass on the sintering and microwave dielectric properties of 0.83$ZnAl_2O_4$-0.17TiO_2, Mater. Res. Bull. 43 (2008) 843-851.
[34] F. Liu, X. Huang, J. Qu, C. Yuan, G. Chen, R. Ma, Crystallization behavior, densification and microwave dielectric properties of MgO-Al_2O_3-SiO_2-TiO_2 system glass-ceramics containing V_2O_5, J. Non-Cryst. Solids. 481 (2018) 329-334.
[35] Y. Shang, C. Zhong, H. Xiong, X. Li, H. Li, X. Jian, Ultralow-permittivity glass /Al_2O_3 composite for LTCC applications, Ceram. Int. 45 (2019) 13711-13718.
[36] J. Xi, G. Chen, F. Liu, F. Shang, J. Xu, C. Zhou, C. Yuan, Synthesis, microstructure and characterization of ultra-low permittivity CuO–ZnO–B_2O_3–Li_2O glass/Al_2O_3 composites for ULTCC application, Ceram. Int. 45 (2019) 24431-24436.
[37] J. Xi, B. Lu, J. Chen, G. Chen, F. Shang, J. Xu, C. Zhou, C. Yuan, Ultralow sintering temperature and permittivity with excellent thermal stability in novel borate glass-ceramics, J. Non-Cryst. Solids. 521 (2019).
[38] Y. Zhang, H. Wu, Crystal structure and microwave dielectric properties of $La_2(Zr_{1-x}Ti_x)_3(MoO_4)_9$ ($0 \leq x \leq 0.1$) ceramics, J. Am. Ceram. Soc. 102 (2019) 4092-4102.
[39] H. Guo, D. Zhou, W. Liu, L. Pang, D. Wang, J. Su, Z. Qi, Microwave dielectric properties of temperature□stable zircon□type (Bi, Ce)VO_4 solid solution ceramics, J. Am. Ceram. Soc. 103 (2019) 423-431.
[40] Y. Zhang, J. Sun, N. Dai, Z. Wu, H. Wu, C. Yang, Crystal structure, infrared spectra and microwave dielectric properties of novel extra low-temperature fired $Eu_2Zr_3(MoO_4)_9$ ceramics, J. Eur. Ceram. Soc. 39 (4) (2019) 1127-1131.

Table 1. Specific compositions of LMZBS composites.

Li_2CO_3	MgO	ZnO	H_3BO_3	SiO_2
15	25	10	50	5

Table 2. Microwave dielectric properties, density and sintering temperature of compounds in composites.

composites	ε_r	$Q\times f$(GHz)	τ_f(ppm/□)	ρ (g/cm3)	ST(℃)	Ref.
Monocelsian	6.9	61290	-40.3	3.390	>1500	This work
$Mg_2B_2O_5$	6.2	32100	-46.0	2.910	1280	15
Li_2ZnSiO_4	5.8	14700	-96.6	3.510	1250	16

Table 3. The microwave dielectric properties of typical low dielectric constant materials

Chemical composition	ST(℃)	ε_r	$Q\times f$	τ_f	Ref.
$Ba_{0.95}Ca_{0.05}Al_2Si_2O_8$	1425	6.7	24335	-19.3	1
$BaAl_2Si_2O_8$-$Ba_5Si_8O_{21}$	750	7.6	12410	-1.2	30
CMS+15wt%LMZBS	900	8.2	32000		14
La_2O_3-B_2O_3-Al_2O_3+40wt%Al_2O_3	900	7.9	3820		31
Li_2O-MgO-ZnO-B_2O_3-SiO_2+5wt%Al_2O_3	900	6.8	12500	-45.0	32
0.83$ZnAl_2O_4$-0.17TiO_2+10wt%BBSZ	950	10.9	12000	-23.2	33
MgO-Al_2O_3-SiO_2-TiO_2+30wt%V_2O_5	950	3.8	12520	-54.0	34
KABS-40wt%ZBS	850	4.9	6873	5.5	35
CuO-ZnO-B_2O_3-Li_2O+10 wt%Al_2O_3	640	3.8	38557	0	36
CuO-ZnO-B_2O_3-Li_2O	620	3.3	17724	0	37
$La_2(Zr_{0.92}Ti_{0.08})_3(MoO_4)_9$	750	10.3	80658	3.5	38
$Bi_{0.05}Ce_{0.95}VO_4$	950	11.9	22360	6.6	39
$Eu_2Zr_3(MoO_4)_9$	600	10.8	74900	-8.9	40
This work	870	7.3	48926	-48.0	

CMS: $CaMgSi_2O_6$. BBSZ: 27B_2O_3-35Bi_2O_3-6SiO_2-32ZnO.

KABS: K_2CO_3-Al_2O_3-B_2O_3-SiO_2. ZBS: ZnO-B_2O_3-SiO_2.

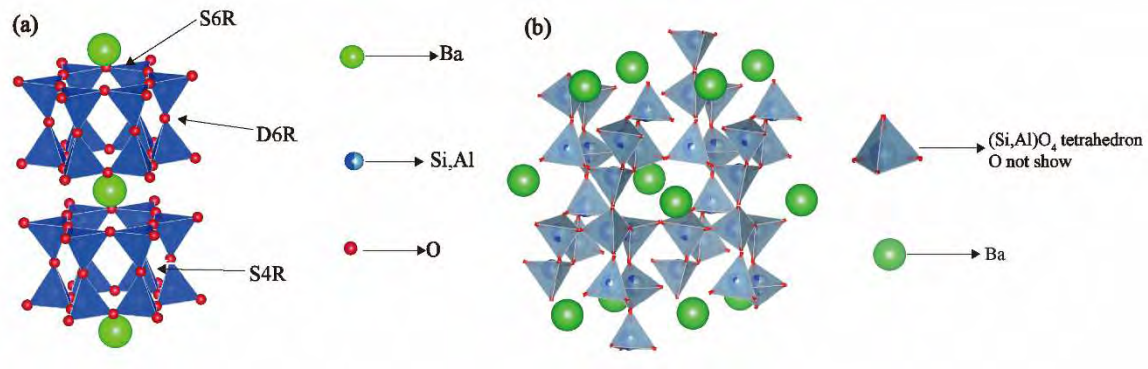

Fig.1. The crystal structure of (a) hexacelsian and (b) monocelsian

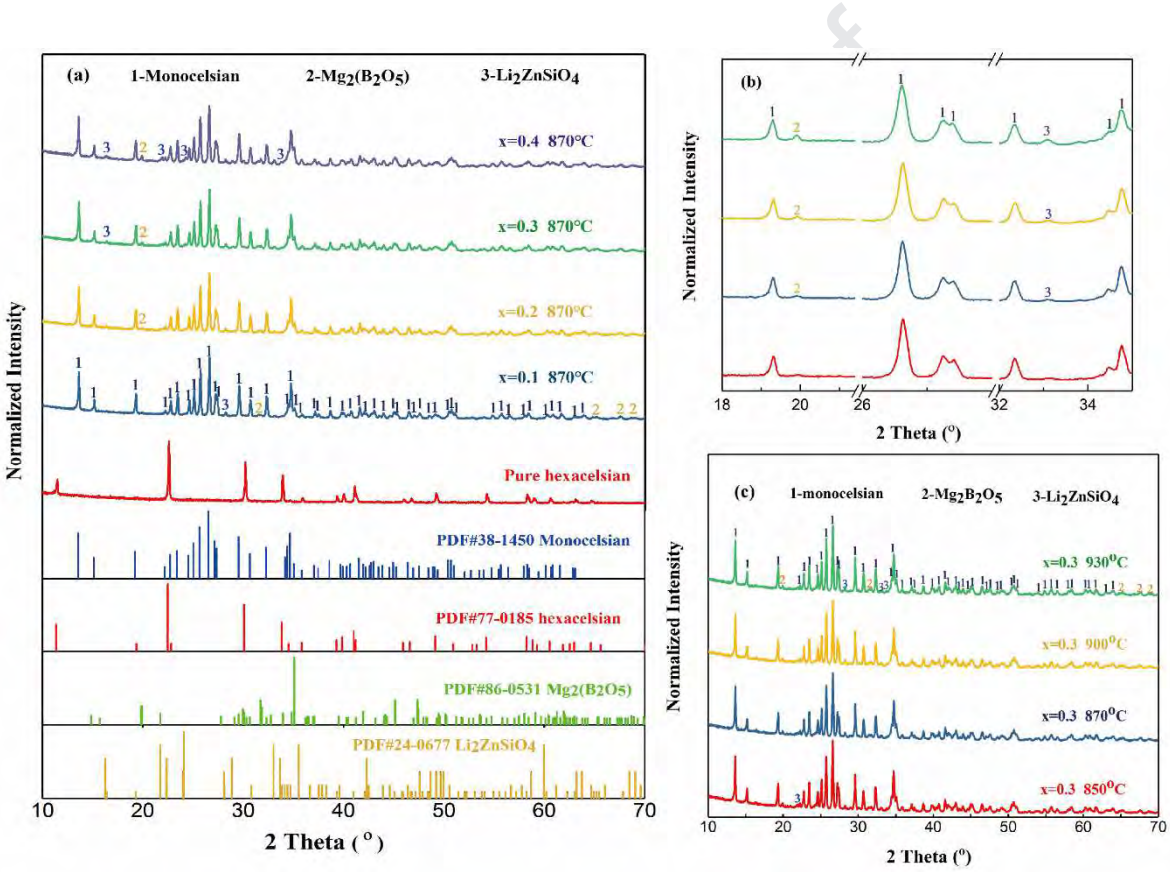

Fig.2. (a) The XRD patterns of BAS with different amount of LMZBS glass sintered at 870 °C for 4 h in air; (b) The XRD patterns of 0.7BAS-0.3LMZBS sintered at 850–930 °C.

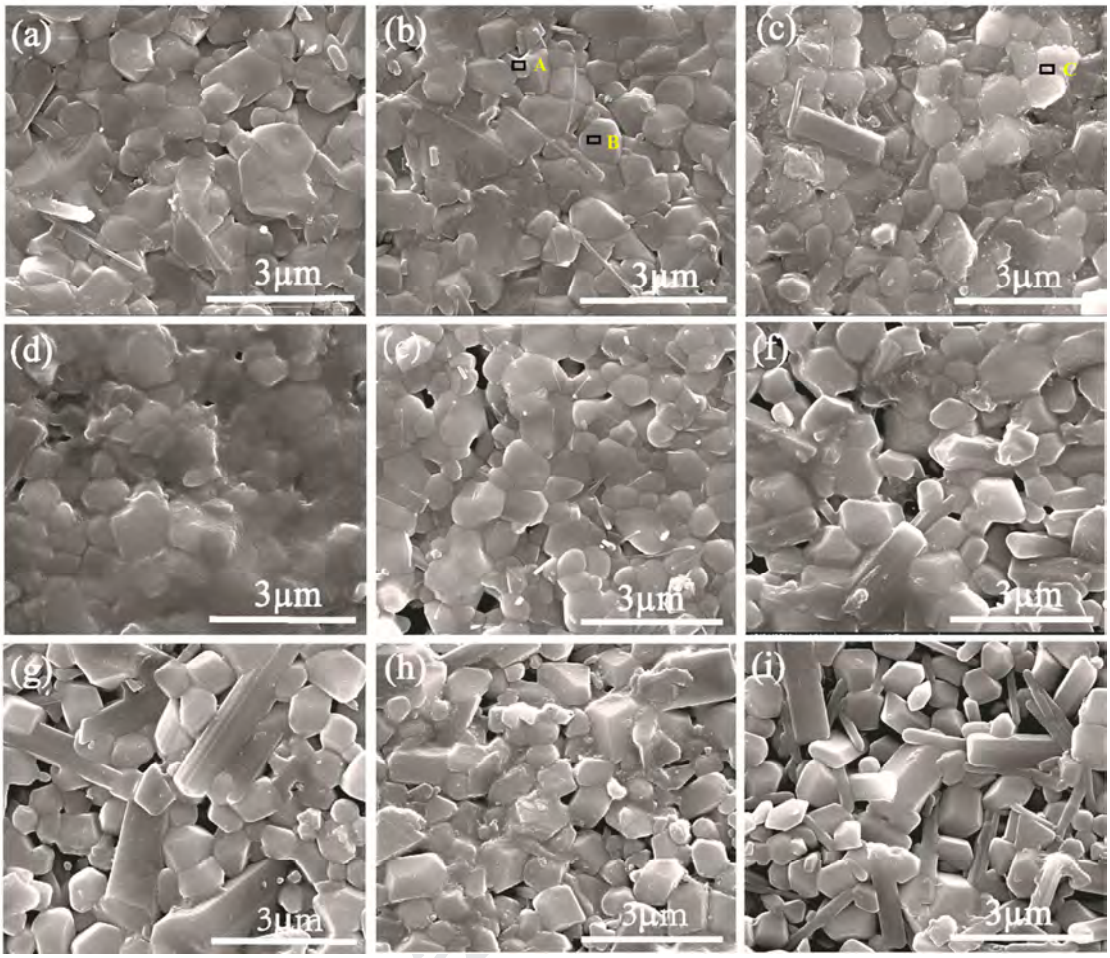

Fig.3. Surface of the (1-*x*)BAS-*x*LMZBS: (a)870 °C, *x*=0.1; (b) 870 °C, *x*=0.2; (c) 870 °C, *x*=0.3; (d) 870 °C, *x*=0.4; (e) 850 °C, *x*=0.3; (f) 900 °C, *x*=0.3; (g) 930 °C, *x*=0.3; (h) 960 °C, *x*=0.3; (i) 990°C, *x*=0.3.

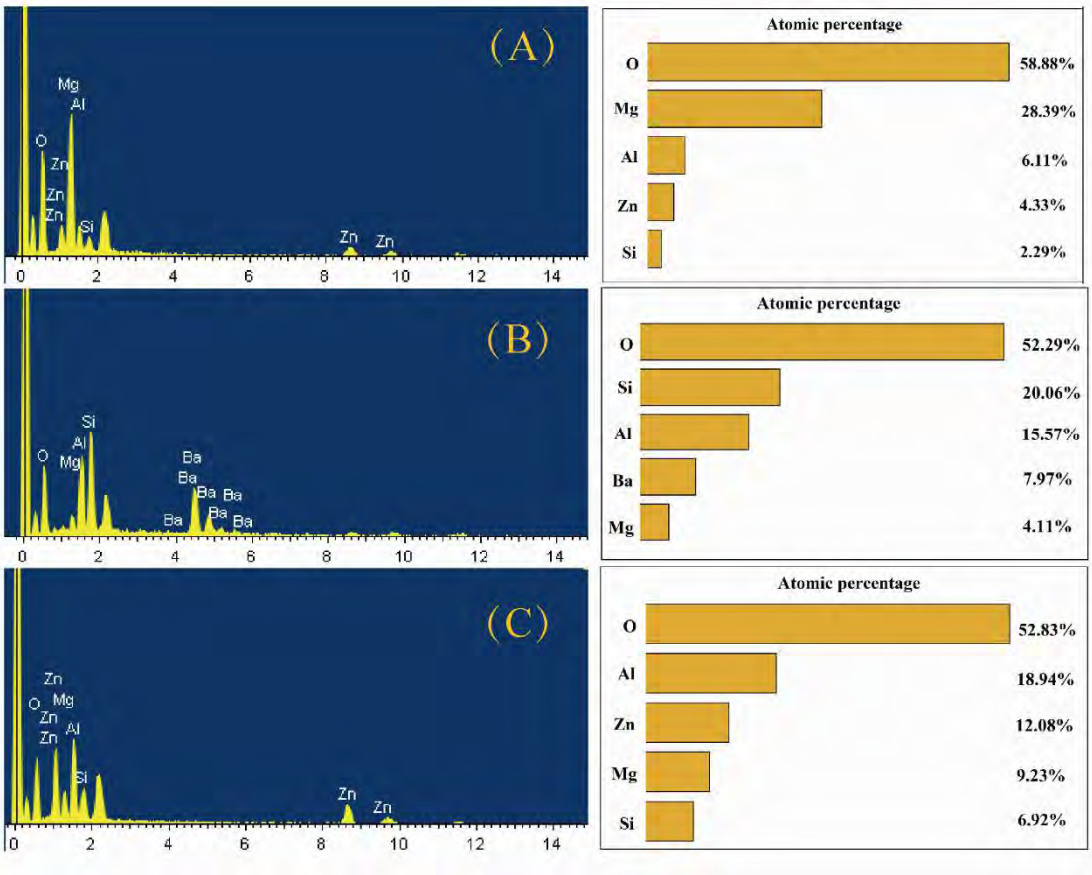

Fig.4. EDS of spot A, B and Spot C

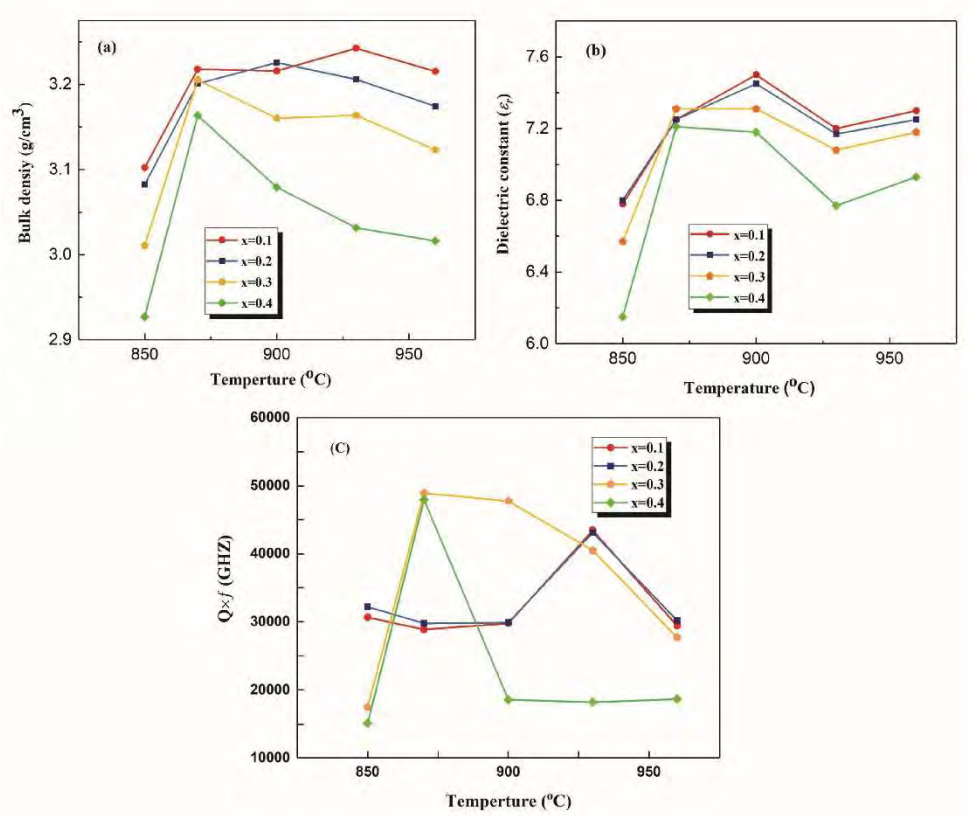

Fig.5. The dielectric property of (1-*x*)BAS-*x*LMZBS: (a) Bulk densities of (1-*x*)BAS-*x*LMZBS(*x*=0.1-0.4) composites sintered at different temperatures; (b) Dielectric constant of (1-*x*)BAS-*x*LMZBS(*x*=0.1-0.4) composites sintered at different temperatures; (c) Q×f value of (1-*x*)BAS-*x*LMZBS(*x*=0.1-0.4) composites sintered at different temperatures.

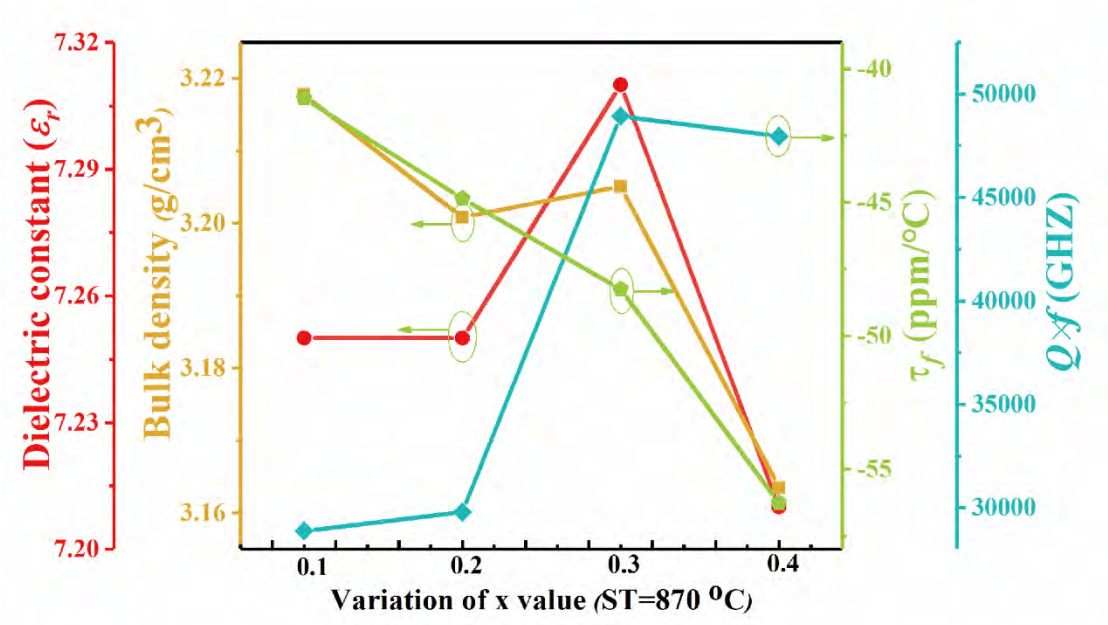

Fig.6. The dielectric properties of (1-x)BAS-xLMZBS sintered at 870□.

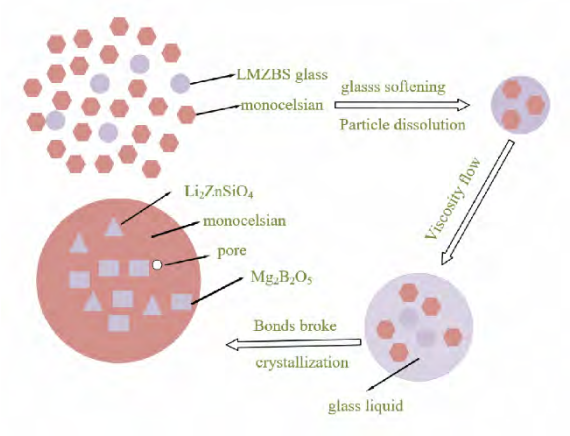

Fig.7. Densification mechanism of BAS/glass composite.

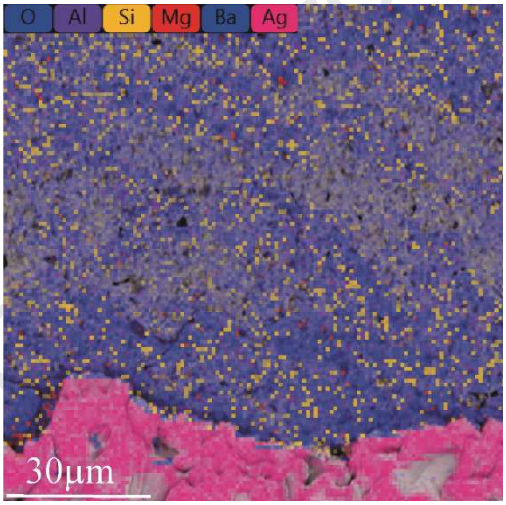

Fig. 8. EDS face scan of the interface between silver electrode and 0.7BAS-0.3LMZBS sintered at 870□ for 4h.

Declaration of interests

The authors declare that they have no known competing financial interests or personal relationships that could have appeared to influence the work reported in this paper.